Far-Infrared dielectric anisotropy and phonon modes in spontaneously CuPt-ordered $Ga_{0.52}In_{0.48}P$

T. Hofmann*
Solid State Physics Group, Faculty of Physics and Geosciences, University of Leipzig, Linnéstraße 5, 04103 Leipzig, Germany

V. Gottschalch
Faculty of Chemistry and Mineralogy, University of Leipzig, Linnéstraße 3, 04103 Leipzig, Germany

M. Schubert†
Center for Microelectronic and Optical Materials Research, Department of Electrical Engineering, University of Nebraska-Lincoln, Lincoln, Nebraska 68588
and Solid State Physics Group, Faculty of Physics and Geosciences, University of Leipzig, Linnéstraße 5, 04103 Leipzig, Germany
(Received 3 April 2002; revised manuscript received 25 June 2002; published 11 November 2002)

The phonon properties of partially $CuPt_B$-ordered $Ga_{0.52}In_{0.48}P$ with degrees of ordering $\eta = 0, 0.19, 0.28, 0.35, 0.47$, determined from generalized ellipsometry measurement of the near-band-gap order birefringence, are studied by far-infrared spectroscopic ellipsometry. We determine precise spectra of the anisotropic dielectric functions. With increasing η all $Ga_{0.52}In_{0.48}P$ phonon modes split in E- and A_1-type vibrations with polarization perpendicular and parallel to the sublattice ordering direction, respectively, and the mode frequencies shift continuously. We demonstrate here that the alloy-induced modes previously observed in highly disordered $Ga_{0.52}In_{0.48}P$ [Phys. Rev. B **64**, 155206 (2001)] have their origin in the ordered atomic arrangement of alike group-III atoms. We propose far-infrared dielectric anisotropy as a sensitive measure for sublattice ordering in multinary III-V alloys.

DOI: 10.1103/PhysRevB.66.195204 PACS number(s): 72.10.Di, 78.30.Fs, 63.20.−e

I. INTRODUCTION

The III-V semiconductor compound $Ga_{1-x}In_xP$ exhibits, in contrast to its binary constituents, a complex polar lattice resonance behavior.[1–7] For ternary alloys a distinction was made so far between the two extreme where infrared-active phonon mode frequencies vary as a function of the alloy composition: A single band of transverse (TO) and longitudinal (LO) phonon modes, which shift continuously between those of the binary constituents, and which is commonly termed as ''one-mode'' behavior. Accordingly, for the ''two-mode'' behavior, two infrared active phonon bands occur close to the frequencies of the binary constituents. For $Ga_{1-x}In_xP$ the ''two-mode'' behavior is commonly accepted.[2,3,8,9] For $x=0.48$ the alloy can be grown lattice matched to GaAs where extensive Raman studies revealed three common features: the GaP-like LO phonon mode at $\sim 380\ cm^{-1}$, the InP-like LO mode at $\sim 361\ cm^{-1}$, and the InP-like TO band at $\sim 328\ cm^{-1}$. The values for the two LO modes reported from different authors are fairly consistent but scatter for the InP-like TO frequency from 325 to $331\ cm^{-1}$.[3,4,6,10,11] The occurrence of the GaP-like TO mode was observed at $\sim 372\ cm^{-1}$ in far-infrared (fir: $\sim 100\ cm^{-1}$ to $\sim 500\ cm^{-1}$) studies only.[7,8,12] Measurement of the fir response provides convenient access to the active lattice modes through an analysis of the complex dielectric function ϵ, provided the experimental method used owns sufficient sensitivity to both real and imaginary parts of ϵ. Such a technique is spectroscopic ellipsometry (SE), a powerful tool, well known for measurements of thin-film dielectric function spectra, and which is superior to intensity spectroscopy techniques in terms of accuracy and sample information.[13,14]

Besides chemical effects due to alloying, or effects due to lattice-mismatch-induced strain, long-range chemical ordering of alike group-III or group-V atoms can drastically affect the phonon mode frequencies as well as other physical properties such as band-gap energies, electron effective mass parameters, and electrical transport properties.[15] The reduced lattice symmetry in ordered alloys also gives rise to anisotropy and phonon mode splitting.[16,17] We have recently observed that highly disordered (Al)GaInP reveal modes with an extremely small polarity.[7] These alloy-induced modes were not seen before application of fir spectroscopic ellipsometry, and are also unknown from the binary constituents, which where extensively studied in bulk or thin film form by Raman and fir intensity spectroscopy. We demonstrate here for GaInP that these alloy-induced modes have their origin in the newly introduced ''degree-of-freedom'' upon alloying: namely, the ordered atomic arrangement of alike group-III or -V atoms.

The spontaneous arrangement of column-III elements in alternating $\{111\}_B$ planes has been found in many ternary zinc-blende III-V semiconductor alloys (e.g., AlGaAs, InGaAs, and GaInP), and results in partially ordered $CuPt_B$-type structure. Spontaneous ordering in $\{111\}_A$ planes is another possible, but rarely observed ordering type. The stacking direction of the superlattice planes in $CuPt_B$-type ordering is parallel to the $[\bar{1}11]$ or $[1\bar{1}1]$ direction. A perfectly arranged superlattice creates a new trigonal crystal, with threefold rotation axis along $[\bar{1}11]$ or $[1\bar{1}1]$, and the symmetry of a completely ordered alloy is lowered from cubic zinc-blende (T_d) to trigonal (C_{3v}) by the superperiodicity along the ordering direction. In real crystals grown by

nonequilibrium thin-film growth techniques such as molecular beam epitaxy or metal-organic vapor-phase epitaxy (MOVPE), the superlattice arrangement is not perfect. This phenomenon is commonly described upon introducing the ordering parameter η, where η may be treated as the difference between the composition x of the two subsequent sublattice planes $A^{\mathrm{III}}_{x+\eta/2}B^{\mathrm{III}}_{x-\eta/2}C^{\mathrm{V}}/A^{\mathrm{III}}_{x-\eta/2}B^{\mathrm{III}}_{x+\eta/2}C^{\mathrm{V}}$.[15] If the random alloy is nonstoichiometric ($x\neq 0.5$), η can only vary between $0\leqslant\eta/2\leqslant\min\{x,1-x\}$; thus fully $CuPt_B$-type ordered ternary compounds ($\eta=1$) may only be formed for $x=0.5$. But to avoid strain effects in $Ga_{1-x}In_xP$ epilayers grown on the GaAs substrate the experimentalist has to revert to the composition $x=0.48$. For a derivation of the order parameter η, however, it is assumed that $x=0.5$. (One may consider the remaining 0.02 Ga as being located at a group III site randomly.) The term $Ga_{0.52}In_{0.48}P$ is then commonly abbreviated as $GaInP_2$ for simplicity, and the latter is in use for the present work throughout.

Most studies concerning the phonon properties of ordered $GaInP_2$ employed Raman spectroscopy to investigate phonon mode frequencies and selection rules. To the best of our knowledge, only one group used fir reflection and transmission measurements to explore the phonon modes of ordered $GaInP_2$, and no exact measurement of the fir dielectric function has been reported so far.[8,12,18] The features observed for ordered $GaInP_2$ in Raman studies within the range $100\ \mathrm{cm}^{-1}\leqslant\omega\leqslant 600\ \mathrm{cm}^{-1}$ can be summarized as follows[11,19–27]: An ordering induced LO mode emerges at $\sim 354\ \mathrm{cm}^{-1}$. The GaP-like LO mode blueshifts with increasing η. For the InP-like LO mode a shift from $\omega\sim 361\ \mathrm{cm}^{-1}$ toward $\sim 365\ \mathrm{cm}^{-1}$ for $\eta\sim 0.5$ was observed, while the corresponding peak in the Raman spectra becomes broadened.[24,25] The InP-like TO mode is found at approximately $330\ \mathrm{cm}^{-1}$. Alsina *et al.*[24] reported a line-shape sharpening of this phonon mode with increasing η. At $\omega\sim 205\ \mathrm{cm}^{-1}$ a folded longitudinal-acoustic-phonon mode has been observed and additional weak modes at $\omega\sim 315$ and $\sim 340\ \mathrm{cm}^{-1}$ were reported by Mintairov and Melehin[23].

SE at fir wavelengths (fir-SE) is a very sensitive tool for determination of fir active phonon modes as well as of free carrier parameters (see, e.g., Refs. 28–34) for semiconductor alloys in layered structures. This technique is used here as a novelty to determine the phonon modes of CuPt-ordered $GaInP_2$. The fir dielectric function, which follows from a precise line-shape analysis of the fir-SE data, provides the link between the optical sample response and the infrared-active phonon modes. For $\eta>0$ $GaInP_2$ is anisotropic, and the observed birefringence will be traced back to the ordinary and extraordinary dielectric functions, which depend on η. It is the focus of the present work to extract the ordering dependence of the alloy-induced modes (AM) and the GaP- and InP-like modes for partial $CuPt_B$-type ordering, upon an analysis of the far-infrared anisotropic dielectric functions. We will compare and discuss our results with those reported so far from experiment and theory. We propose the fir dielectric anisotropy as sensitive measure for composition and state of ordering in multinary alloys.

II. THEORY

A. Fir model dielectric function

The contributions of polar lattice vibrations to the dielectric function ϵ of semiconductors are commonly described using oscillator functions with Lorentzian-type broadening.[35–37] Ternary alloys with multiple phonon branches such as $GaInP_2$ require sets of multiple oscillators for model presentation of ϵ. The factorized form of the anharmonic Lorentzian-sum presentation is used here for a parametrization of the $GaInP_2$ dielectric function (electric field polarization $j=$ "$\parallel$," "$\perp$" with respect to the ordering direction),[38,39]

$$\epsilon_j^{(\mathrm{L})}(\omega)=\epsilon_{\infty,j}\prod_{i=1}^{\nu}\frac{\omega^2+i\gamma_{\mathrm{LO},ij}\omega-\omega^2_{\mathrm{LO},ij}}{\omega^2+i\gamma_{\mathrm{TO},ij}\omega-\omega^2_{\mathrm{TO},ij}}, \tag{1}$$

where $\omega_{\mathrm{LO},i}$, $\gamma_{\mathrm{LO},i}$, $\omega_{\mathrm{TO},i}$, and $\gamma_{\mathrm{TO},i}$ are the frequency and the broadening values of the ith LO and TO phonons, respectively, and the index i runs over ν modes. Kasic and co-workers[33,34] presented a convenient model for treatment of fir active modes with small polarity within the anharmonic oscillator approximation. This approach was successfully applied to describe the response of low-polarity modes in highly-disordered $GaInP_2$,[7] and is adopted in this work as well. For details and notation we refer to Refs. 33 and 34. The $GaInP_2$ epitaxial layers were grown on Te-doped GaAs substrates. For a correct model description of the fir response of the samples, the contribution of the free carriers within the substrates must be considered. The classical Drude approximation holds with sufficient accuracy for description of contributions from free carriers to ϵ of III-V semiconductors, and relates the free-carrier concentration N, the free-carrier effective mass m^*, and the optical carrier mobility parameter μ to the dielectric function ϵ.[36] Plasmons interact with LO phonons, and LO-phonon-plasmon (LPP) coupling has been observed by fir spectroscopy in n-type GaAs,[40] and also in p-type GaAs.[41] For small plasmon dampings, the LPP mode frequencies can be diverted from the roots of ϵ, which split for n-type GaAs into low frequency (LPP^-) and high-frequency branches (LPP^+).[37] The LPP mode coupling mechanism distinctly affects the fir-response of the samples studied. These effects can be consistently described within the model calculations performed here for the layered sample structures, and are clearly traced back to the free-carrier properties of the substrate materials. Results for the free-carrier parameters obtained thereby for the individual substrates differ slightly, depending on the doping concentration, and parameters are given further below. The free-carrier contributions originating from the substrate do not influence the fir response from the $GaInP_2$ layers studied here. Further discussions of the LPP coupling mechanism is omitted. The interested reader is referred to previous publications devoted to the ellipsometry study and line shape analysis for phonon modes and free-carrier parameters in layered III-V compound materials.[32–34,42–45]

B. Uniaxial dielectric tensor of CuPt-type $GaInP_2$

The dielectric tensor of a completely CuPt-type ordered alloy is optically uniaxial, and may be written in diagonal form as

$$\boldsymbol{\epsilon}(\eta)=\begin{pmatrix} \epsilon_{\perp} & & \\ & \epsilon_{\perp} & \\ & & \epsilon_{\parallel} \end{pmatrix}, \tag{2}$$

where $\epsilon_{\perp}$ and $\epsilon_{\parallel}$ denote the ordinary and extraordinary dielectric functions for polarizations perpendicular and parallel to the ordering direction, respectively. The optical axis is parallel to the ordering direction, which is tilted from the sample normal by $\Theta=54.7°$. For $0<\eta<1$ we assume $\boldsymbol{\epsilon}(\eta)$ as the uniaxial dielectric tensor, which describes a single homogeneous ordered phase. This implies that we assume ordering as a single subvariant only, i.e., ordering takes place in one of the two possible [111]-type directions. For assignment, and without loss of generality, we choose the $[\bar{1}11]$ direction. We observed that for the partially ordered samples, the optical response is that of a uniaxial material, with the optical axis collinear to the $[\bar{1}11]$ direction. For perfect CuPt-type ordering, the zinc-blende lattice modes should split into modes with A and E_1 symmetries, and with lattice displacement patterns parallel and perpendicular to the trigonal axis, respectively. For $0<\eta<1$ the trigonal lattice is not perfect but the ordering axis is clearly defined. The dielectric tensor is found to be uniaxial from the fir ellipsometry experiment. We therefore keep the symbol assignment for the uniaxial phonon modes found with polarization parallel (A_1) and perpendicular (E) to the optical axis, and which we derive from $\epsilon_{\parallel}$ and $\epsilon_{\perp}$, respectively.

Alsina *et al.*[12] attempted to decompose $\boldsymbol{\epsilon}(\eta)=(1-\eta^2)\boldsymbol{\epsilon}_{\rm dis}+\eta^2\boldsymbol{\epsilon}_{\rm ord}$, where $\boldsymbol{\epsilon}_{\rm dis}$ is isotropic and represents a disordered phase, and $\boldsymbol{\epsilon}_{\rm ord}$ is the tensor for perfect ordering. This assignment is leaning on the η^2 rule, where all physical quantities induced upon ordering should scale accordingly.[15] We find, however, that $\boldsymbol{\epsilon}(\eta)$ is uniaxial with no isotropic (disordered) part for $\eta>0$. Also, the η range studied here does not allow one to predict $\boldsymbol{\epsilon}(\eta=1)$, which is completely unknown, and at this point the approach pursued by Alsina *et al.*[12] seeamed in appropriate to us.

C. SE data analysis

Ellipsometry determines the complex reflectance ratio ρ

$$\rho\equiv\frac{r_p}{r_s}=\tan\Psi e^{i\Delta}, \tag{3}$$

where r_p and r_s are the complex Fresnel reflection coefficients for light polarized parallel (p) and perpendicular (s) to the plane of incidence, respectively.[13] Ψ and Δ denote the standard ellipsometric parameters. Ψ and Δ, measured on layered samples, depend on all materials' dielectric functions including their directional dependencies (anisotropy), layer thickness values, and the incident wavelength. In general, stratified layer model calculations are needed for SE data analysis (see Jellison,[14] and references therein). Models must invoke appropriate physical relationships, which must render the dielectric response studied. Materials' physical quantities, such as frequencies, amplitudes, and broadening parameters of polar lattice resonances, then follow through a modeling of all materials' $\boldsymbol{\epsilon}$ spectra. Parameters with significance are varied during data analysis until calculated and measured data match as close as possible (best-fit). Least-square approaches, which minimize weighted test functions (maximum likelihood methods), such as the Levenberg-Marquardt algorithm,[46] are employed for fast convergence. Detailed discussions on parameter correlation issues, proper data noise treatment, and ''best-choice-fitting'' procedures in ir ellipsometry data analysis for semiconductor layer structures can be found in Refs. 30, 33, and 47, and references therein.

The model used here accounts for the layer sequence substrate/buffer/epilayer, where substrate and buffer are treated isotropic. The epilayer is modelled as uniaxial layer for $\eta>0$, or as isotropic layer for $\eta=0$, respectively.[48] The MDF described in Ref. 7 is used to calculate $\boldsymbol{\epsilon}$ for the n-type Te-doped GaAs substrate [Eq. (1), $\nu=1$, and Eq. (3) and (4) with $m^*=0.067m_e$ for GaAs], and the undoped GaAs buffer [Eq. (1), $\nu=1$] with $\omega_{\rm TO}=267.7\ {\rm cm}^{-1}$, $\omega_{\rm LO}=291.3\ {\rm cm}^{-1}$, $\gamma_{\rm TO}=\gamma_{\rm LO}=5.6\ {\rm cm}^{-1}$, and $\epsilon_{\infty}=11.0$, common to both substrate and buffer.[49] N and μ need to be varied, and account for the free-carrier response within the substrate. The thickness of the buffer layer $d_{\rm buffer}$ is also an adjustable parameter of significance. To extract $\boldsymbol{\epsilon}(\eta)$ of the $GaInP_2$ layers, two sets of MDF equations [Eqs. (1) and (2) in Ref. 7 with $\nu=2, m\leqslant 3$] for $\epsilon_{\perp}$ and $\epsilon_{\parallel}$ were used, adjusting all corresponding MDF parameters separately. This approach provides sufficient sensitivity to the $GaInP_2$ layer thickness d, the substrate free-carrier parameters N and μ, and the buffer layer thickness $d_{\rm buffer}$. The best-fit results of d, $d_{\rm buffer}$, N, and μ are given in Table I.

D. Estimation of the degree of ordering

CuPt-ordering cause reduction of the fundamental band gap $\Delta E_g^{(\eta)}=E_g^{(\eta)}-E_g^{(\eta=0)}$, and top-level valence-band splitting δE_{ij} at $k=0$ (Γ point).[50–53] The δE_{ij}'s have been related by Wei and Zunger[51] to the degree of ordering η upon the amount of spin-orbit and crystal field splitting parameters within the quasicubic perturbation model, as well as to the amount of order induced band gap reduction.[51,54,55] Generalized variable angle spectroscopic ellipsometry (gVASE) at near-infrared to visible wavelengths (nir-vis: 1650–500 nm) can be employed to determine the fundamental band-to-band transitions $E_0^{(1)}$, $E_0^{(2)}$, and $E_0^{(3)}$ from the $\Gamma_{4,5v}$, $\Gamma_{6(1)v}$, and $\Gamma_{6(2)v}$ valence band states to the Γ_{6c} conduction band states at $k=0$ from the nir-vis dielectric functions $\epsilon_{\parallel}$ and $\epsilon_{\perp}$ as is described in detail in Ref. 58. For detailed discussion of the model-line shape analysis of the CuPt-ordering-induced order-birefringence measured by the gVASE approach at visible wavelengths the reader is referred to Refs. 53 and 58–60.

III. EXPERIMENT

The $GaInP_2$ films were grown by MOVPE on (001) GaAs with several substrate orientation defects (column 3 in Table

TABLE I. Best-fit results for $GaInP_2$ layer thickness d, GaAs buffer layer thickness d_{buffer}, and the GaAs substrate free carrier parameters obtained from the fir-SE data analysis. The error limits, which correspond to 90% reliability are given in parentheses.

No.	d (nm)	d_{buffer} (nm)	N(300 K) (10^{17} cm^{-3})	μ [10^3 cm^2/(Vs)]	LPP$^-$ (cm^{-1})	LPP$^+$ (cm^{-1})
1	1286(5)	161(7)	3.5(0.03)	2.88(0.07)	169	307
2	384(5)	130(5)	3.7(0.03)	2.63(0.06)	172	308
3	404(5)	130(5)	3.8(0.03)	2.57(0.06)	175	309
4	375(5)	137(4)	5.9(0.03)	2.53(0.06)	208	325
5	1463(3)	130(5)	3.5(0.03)	2.76(0.06)	167	307

II). Prior to the $GaInP_2$ layers a GaAs-buffer layer with a thickness of $d_{\text{buffer}} \sim 150$ nm was deposited. The substrates were Te doped whereas all epitaxial layers were intentionally undoped. The sample growth parameters are summarized in Table II. Room temperature fir-SE measurements for wavenumbers from 100 cm^{-1} to 600 cm^{-1}, and with a resolution of 1 cm^{-1} were carried out using a prototype, rotating-analyzer, Fourier-transform-based ellipsometer, which was equipped with a He-cooled bolometer detector system. For each sample we performed measurements at two different sample orientations.

(a) A $[\bar{1}10]$ axis parallel to the plane of incidence (setup $\mathcal{A}$); the ordering axis is located within the plane of incidence,

(b) A $[\bar{1}10]$ axis perpendicular to the plane of incidence (setup $\mathcal{B}$); the ordering axis is located within the plane perpendicular to the plane of incidence.

All fir-SE measurements were carried out at 70° angle of incidence ϕ_a.[61] To determine the degree of ordering η, room temperature nir-vis gVASE and standard SE measurements in the spectral range from 0.75 to 2.5 eV were performed for each sample with a resolution of 0.01 eV at two angles of incidence ($\phi_a = 15°$ and 65°) in reflection arrangement. Experimental and best-fit spectra are shown exemplarily for sample 5 in Fig. 1.

TABLE II. Sample parameters of the $GaInP_2$ layers studied in this work. The growth parameters (growth temperature T_g and substrate orientation) have been varied to obtain different degrees of ordering η. The values of E_g and ΔE_{VBS} are determined by nir-vis gVASE as described in Ref. 58, and are given in columns 5 and 6, respectively. The degree of ordering η was calculated using Eq. (7) of Ref. 54 and the maximum band-gap reduction parameter of $\Delta E_g = 490$ meV given in Refs. 56 and 57.

No.	T_g (°C)	Orientation	$\Delta a/a$ (10^{-4})	E_g (eV)	ΔE_{VBS} (meV)	η
1	595	2°(111)Ga	−4	1.900	∼0	∼0
2	720	6°(111)Ga	15	1.885	3.8	0.19
3	650	6°(111)Ga	7	1.866	8.0	0.28
4	720	6°(111)As	∼0	1.847	12.2	0.35
5	680	2°(111)Ga	∼0	1.805	20.6	0.47

IV. RESULTS AND DISCUSSION

In the following sections we present the fir-SE spectra for the most ordered sample (Figs. 2 and 3), the corresponding anisotropic MDF of the $GaInP_2$ layer (Fig. 4), and the fir-SE spectra for all samples (Fig. 5 and 6). The phonon mode behavior for $GaInP_2$ is given as a function of the ordering

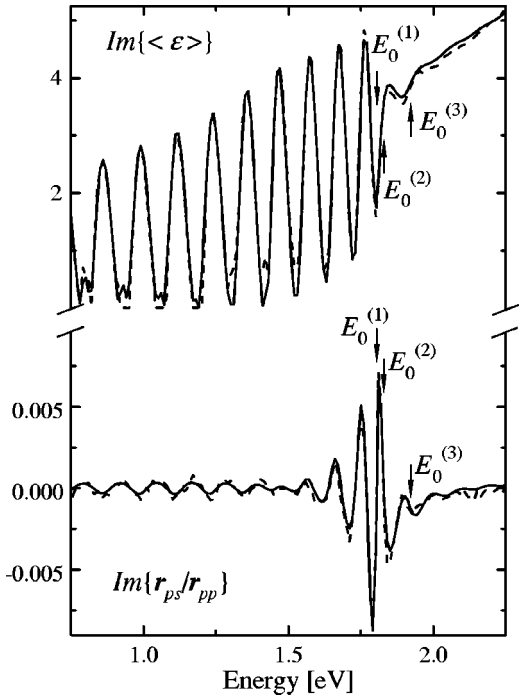

FIG. 1. Imaginary part of the pseudodielectric function $\langle \epsilon \rangle$ of CuPt-type ordered $GaInP_2$ (sample 5 in Table II), obtained from a single-angle-of-incidence standard rotating-analyzer ellipsometry measurement at fixed incident polarization ($\phi_a = 65°$; polarizer at 45° azimuth; dashed line: experimental data; solid line: best-fit). Also shown are reflection gVASE data $Im\{r_{ps}/r_{pp}\}$ obtained at $\phi_a = 15°$, for example. The gVASE data reveal the birefringence of the $GaInP_2$ epilayer due to the CuPt-type superlattice ordering. The energies of the band-to-band transitions $E_0^{(1)}$, $E_0^{(2)}$, and $E_0^{(3)}$ from the $\Gamma_{4,5v}$, $\Gamma_{6(1)v}$, and $\Gamma_{6(2)v}$ valence band states to the Γ_{6c} conduction band states at $k = 0$ follow from model-line shape analysis of the order-birefringence. [After Schubert *et al.* (Ref. 58).] The transition energies $E_0^{(1)}$, $E_0^{(2)}$, and $E_0^{(3)}$ are then related to the degree of ordering η through the quasicubic model approximation and its ordering dependence. [After Wei *et al.* (Ref. 54).]

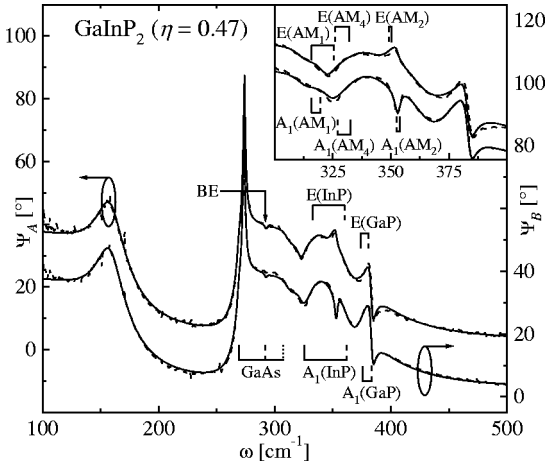

FIG. 2. Experimental (dashed line) and calculated (solid line) fir-SE Ψ spectra at $\phi_a = 70°$ for sample 5. $\Psi_{\mathcal{A}}$ and $\Psi_{\mathcal{B}}$ denote spectra taken with the sample $[\bar{1}10]$ axis parallel and perpendicular to the plane of incidence, respectively. The $\Psi_{\mathcal{A}}$ spectrum is shifted by 15° for convenience. The reststrahlen band of the *n*-type Te-doped GaAs substrate extends between $\omega_{TO} \sim 268$ cm^{-1} (solid vertical line) and LPP$^+ \sim 307$ cm^{-1} (dotted vertical line). The small dip very close to the GaAs LO mode at $\omega_{LO} \sim 292$ cm^{-1} (dashed vertical line) is due to the Berreman effect (BE) caused by the undoped GaAs buffer layer (Refs. 62 and 64). The GaInP$_2$ InP-, and GaP-like TO (solid vertical lines) and LO (dotted vertical lines) modes are indicated by brackets. The inset enlarges the spectral region of AM$_1$, AM$_2$, and AM$_4$.

parameter η (Figs. 7 and 8), and is compared with data reported previously.

A. FIR-SE

The best-fit spectra where obtained through the MDF approach described in Sec. II. The uniaxial character of the material is reflected by the differences in the Ψ and Δ spectra of the two orientations (setups $\mathcal{A}$ and $\mathcal{B}$). A simultaneous analysis of the two fir-SE data sets enables us to extract the $\epsilon_{\parallel}$ and $\epsilon_{\perp}$ spectra of the GaInP$_2$ layers. Figure 2 shows the experimental (dashed line) and calculated (solid line) fir-SE

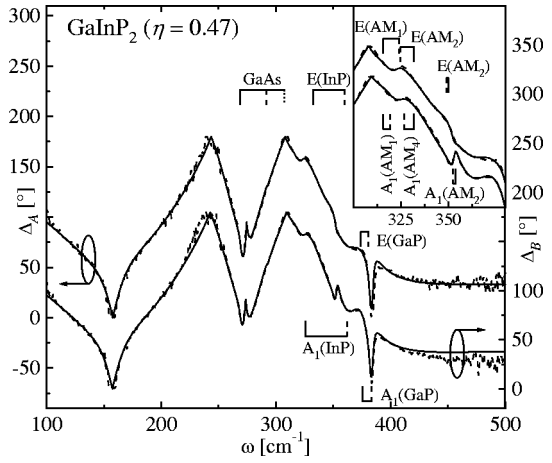

FIG. 3. Same as Fig. 3 for Δ spectra.

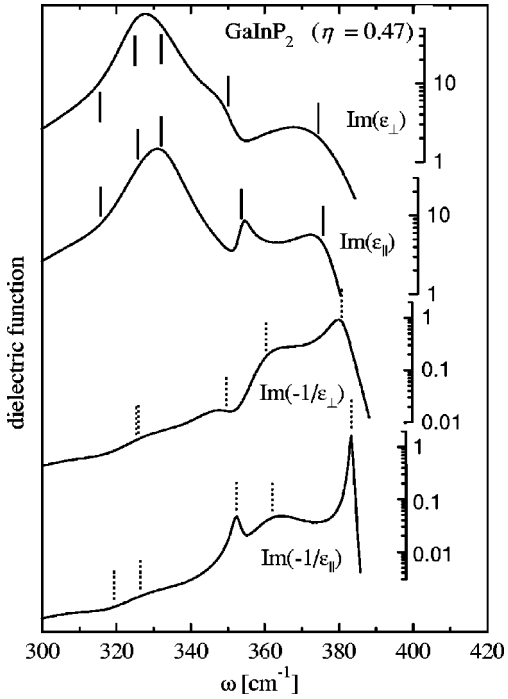

FIG. 4. GaInP$_2$ MDF's $\epsilon_{\parallel}$ and $\epsilon_{\perp}$ obtained from the best-fit fir-SE data analysis for sample 5 with $\eta = 0.47$. Spectrally local maxima of Im($\epsilon_{\perp}$) and Im($\epsilon_{\parallel}$) coincide with the spectral position of the E(TO) and A_1(TO) mode parameter frequencies, which are indicated with vertical solid lines, respectively. The corresponding LO mode frequencies are located near maxima of Im($-1/\epsilon_{\perp}$) and Im($-1/\epsilon_{\parallel}$), and are marked with vertical dotted lines. The best-fit values for the GaInP$_2$ MDF parameter for sample 5 are given in Table III.

Ψ spectra for sample 5 with $\eta = 0.47$. The spectra measured with the sample $[\bar{1}10]$ axis parallel (setup $\mathcal{A}$) and perpendicular ($\mathcal{B}$) to the plane of incidence are denoted by $\Psi_{\mathcal{A}}$ and $\Psi_{\mathcal{B}}$, respectively. The corresponding fir-SE Δ spectra are shown in Fig. 3.

The reststrahlen band of the *n*-type GaAs can be recognized in the spectral region between $\omega_{TO} \sim 268$ cm^{-1} and $\omega_{LPP^+} \sim 307$ cm^{-1}. The uncoupled GaAs LO phonon mode causes the Berreman effect at $\omega_{LO} \sim 292$ cm^{-1}.[62–66] Two strong peaks can be recognized at $\omega \sim 155$ and 273 cm^{-1}. Both resonances are attributed to plasmon-phonon-mode-induced *s*-polarized surface-bound electromagnetic wave propagation parallel to the substrate/buffer interface, which cause resonant losses of the *s*-polarized reflectivity.

The GaInP$_2$ layer imposes distinct structures in the fir-SE Ψ spectra for 310 cm$^{-1} \leqslant \omega \leqslant 400$ cm^{-1}. The InP- and GaP-like TO (LO) phonon modes, obtained from the best-fit analysis, are indicated by solid (dashed) vertical lines. We observe small frequency differences for the E- and A_1-type phonon modes. The differences between the $\Psi_{\mathcal{A}}$ and $\Psi_{\mathcal{B}}$ spectra can be appreciated in the spectral region 310 cm^{-1} $< \omega <$ 360 cm^{-1}. To reproduce the experimental line shape in this spectral region properly we included three alloy-induced modes AM$_1$, AM$_2$, and AM$_4$.[67] These modes have different TO-LO splitting values and are clearly anisotropic as seen from Figs. 2 and 3. The TO (LO) phonon mode

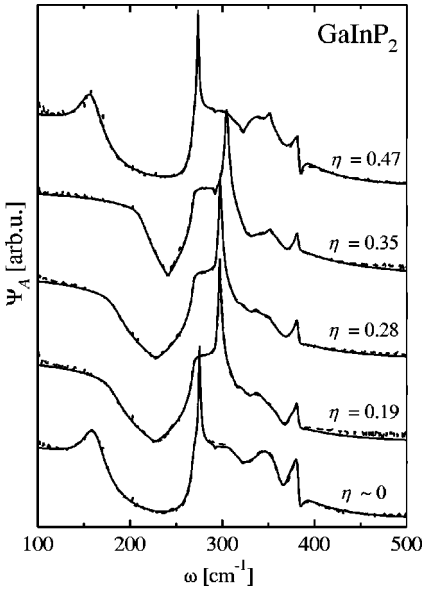

FIG. 5. Experimental (dashed line) and calculated (solid line) fir-SE Ψ spectra at a 70° angle of incidence for all samples investigated in this work. All Ψ spectra were obtained with sample $[\bar{1}10]$ axis parallel to the plane of incidence (setup $\mathcal{A}$; see Sec. III). The strong difference between the Ψ spectra in the region $150\ \mathrm{cm}^{-1} \leqslant \omega \leqslant 310\ \mathrm{cm}^{-1}$ reflect the different doping levels and carrier mobilities of the *n*-type Te-doped GaAs substrates.

frequency parameters are indicated by dashed (solid) vertical lines (see also the inset in Figs. 2 and 3). At approximately $350\ \mathrm{cm}^{-1}$ one can recognize a sharp maximum and minimum in $\Psi_{\mathcal{A}}$ and $\Psi_{\mathcal{B}}$, respectively. Here occurs AM_2, the strongest AM mode, which has been often observed in the literature and which has already been attributed to CuPt ordering.[8,11,12,18,21–25,27] The *E*-type AM_2 shows a small TO-LO splitting ($\sim 0.4\ \mathrm{cm}^{-1}$) in comparison to the larger

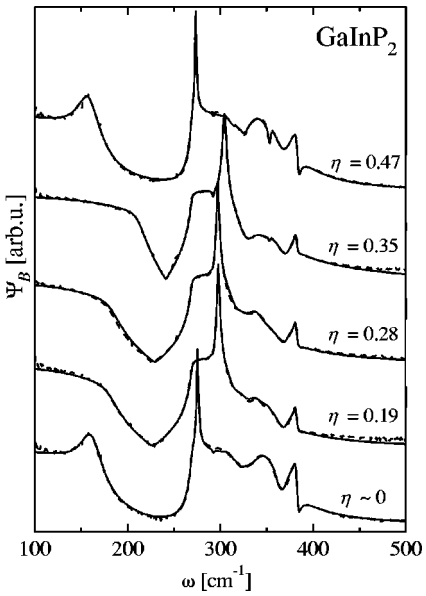

FIG. 6. Same as Fig. 6 for the sample $[\bar{1}10]$ axis perpendicular to the plane of incidence (setup $\mathcal{B}$; see Sec. III).

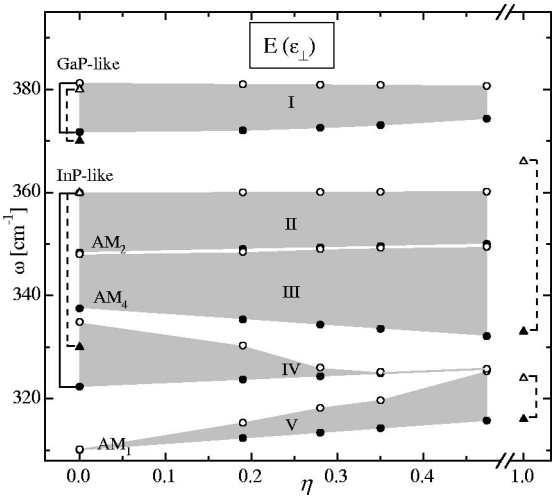

FIG. 7. *E*-type phonon modes versus η (solid symbols: TO; open symbols: LO). We observe five bands (I–V) emphasized by hatched areas. The dashed vertical brackets at $\eta = 0$ and 1 indicate the phonon mode frequencies calculated by Ozoliņš and Zunger (Ref. 17) for random and perfectly ordered GaInP_2, respectively. Note the abscissa break at $\eta \sim 0.49$.

value for $A_1(\mathrm{AM}_1)$ ($\sim 1.5\ \mathrm{cm}^{-1}$). This leads to a strong anisotropy and causes the main difference between $\Psi_{\mathcal{A}}$ and $\Psi_{\mathcal{B}}$. AM_1 and AM_4 contribute further subtle differences between $\Psi_{\mathcal{A}}$ and $\Psi_{\mathcal{B}}$ in the spectral range $310\ \mathrm{cm}^{-1} < \omega < 340\ \mathrm{cm}^{-1}$.

All phonon modes obey the "alternation rule."[35] Note that AM_2 and AM_4 are located within the InP-like phonon band and the sequence $\omega_{TO}^{\mathrm{InP}} < \omega_{LO}^{\mathrm{AM}_4} < \omega_{TO}^{\mathrm{AM}_4} < \omega_{LO}^{\mathrm{AM}_2} < \omega_{TO}^{\mathrm{AM}_2} < \omega_{LO}^{\mathrm{InP}}$ fulfills the "TO-LO alternation rule" for both A_1- and *E*-type modes.[33]

Figure 4 presents the GaInP_2 best-fit MDF for $\epsilon_{\parallel}$ and $\epsilon_{\perp}$ for sample 5 and the obtained best-fit MDF parameter for this sample are summarized in Table III. The $E(\mathrm{TO})$ $[A_1(\mathrm{TO})]$ phonon modes can be recognized as peaks in $\mathrm{Im}(\epsilon_{\perp})$ $[\mathrm{Im}(\epsilon_{\parallel})]$ whereas $\mathrm{Im}(-1/\epsilon_{\perp})$ $[\mathrm{Im}(-1/\epsilon_{\parallel})]$ peak near the $E(\mathrm{LO})$ $[A_1(\mathrm{LO})]$ phonon mode frequencies. The

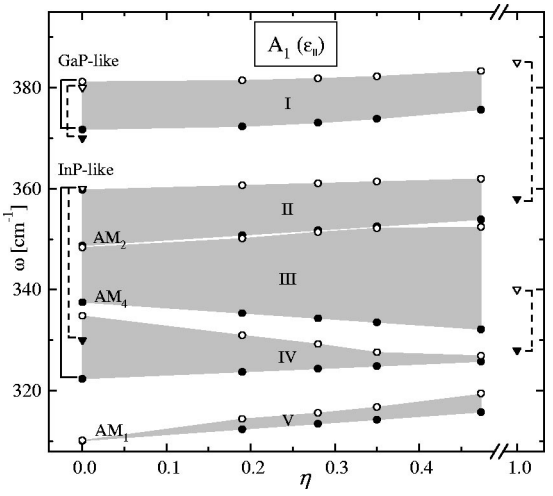

FIG. 8. Same as Fig. 7 for the A_1-type phonon modes.

TABLE III. Best-fit results for the $GaInP_2$ MDF parameter in Eq. (2) of Ref. 7 for sample 5 obtained from the fir-SE data analysis (all values in cm^{-1}). The error limits, which correspond to 90% reliability are given in parentheses. Note that $\omega_{LO}^{AM,k}=\omega_{TO}^{AM,k}-\delta^{AM,k}$ is used (see Ref. 7 for symbol notation).

		ω_{TO}	ω_{LO}	γ_{TO}	γ_{LO}
	$\epsilon_\perp$	325.8(2.1)	360.2(0.6)	14.5(0.7)	14.4(0.5)
InP	$\epsilon_\parallel$	325.8(1.5)	362.0(0.5)	23.5(3.0)	16.7(0.4)
	$\epsilon_\perp$	374.3(0.5)	380.7(0.5)	21.3(0.6)	5.9(0.2)
GaP	$\epsilon_\parallel$	375.6(0.4)	383.3(0.5)	12.9(0.4)	1.0(0.2)
		ω_{TO}	$\delta\omega$	γ_{TO}	$\delta\gamma$
	$\epsilon_\perp$	315.7(2.0)	9.7(6.1)	60.0(1.5)	−11.5(65.4)
AM_1	$\epsilon_\parallel$	315.7(1.0)	3.8(1.1)	49.2(4.6)	−18.1(2.9)
	$\epsilon_\perp$	350.0(1.5)	−0.5(1.7)	10.7(1.1)	6.8(2.2)
AM_2	$\epsilon_\parallel$	353.9(0.4)	−1.5(0.6)	3.4(0.2)	−0.9(0.2)
	$\epsilon_\perp$	332.1(2.1)	−6.3(6.2)	20.9(1.6)	26.2(67.3)
AM_4	$\epsilon_\parallel$	332.1(1.9)	−5.2(2.0)	15.3(1.3)	42.5(4.9)

solid and dashed vertical lines in Fig. 4 indicate the TO and LO phonon mode parameter frequencies, respectively. The mode assignment with E- or A_1-type symmetry follows from parameters taken from the MDF's $\epsilon_\parallel$ and $\epsilon_\perp$, respectively, as mentioned in Sec. II B. It is obvious that $\mathrm{Im}(\epsilon_\perp)$ $[\mathrm{Im}(\epsilon_\parallel)]$ differ particularly in the region around $\omega\sim350$ cm^{-1}, where only in $\mathrm{Im}(\epsilon_\parallel)$ a peak is noticeable. This peak corresponds to the A_1(TO) resonance of the AM_2 mode. Note that Alsina *et al.*[12] concluded a similar behavior of $\epsilon_\parallel$ from polarized fir reflection studies of $GaInP_2$, although a much less accurate line shape analysis was presented there (see Fig. 7 in Ref. 12). Comparing $\mathrm{Im}(-1/\epsilon_\perp)$ and $\mathrm{Im}(-1/\epsilon_\parallel)$ one can observe here that $\mathrm{Im}(-1/\epsilon_\parallel)$ also peaks in the region $\omega\sim350$ cm^{-1} but only a broad structure can be noticed in this region in $\mathrm{Im}(-1/\epsilon_\perp)$. The peak in $\mathrm{Im}(-1/\epsilon_\parallel)$ can be identified as the A_1(LO) resonance of the alloy-induced mode AM_2. The TO-LO splitting and the broadening values of the A_1-type AM_2 mode are smaller than the corresponding parameters of the AM_1 and AM_4 mode. This leads, in contrast to the AM_2, to very broad structures in $\mathrm{Im}(\epsilon_{\perp,\parallel})$ and $\mathrm{Im}(1/\epsilon_{\perp,\parallel})$, and causes subtle differences between $\Psi_{\mathcal{A}}$ and $\Psi_{\mathcal{B}}$ (see Fig. 2) in the spectral range $310\ cm^{-1}<\omega<340\ cm^{-1}$.

The experimental (dashed lines) and calculated (solid lines) fir-SE Ψ spectra for all samples studied in this work are shown in Figs. 5 (setup $\mathcal{A}$) and 6 ($\mathcal{B}$). The Ψ spectra for the various samples differ strongly in the GaAs reststrahlen region because, unintentionally, substrates with slightly different doping levels were used for $GaInP_2$ sample growth. The most obvious effect in the region $310\ cm^{-1}\leqslant\omega\leqslant360\ cm^{-1}$ is the evolution of the additional feature (AM_2) near $\omega\sim350$ cm^{-1} in Ψ (Figs. 5 and 6). More subtle changes in the experimental line shape occur at $\omega\sim315$ and 336 cm^{-1}. However, the spectra are also influenced by the thickness of the GaAs buffer layer, and the thickness of the $GaInP_2$ epilayer, and which must be reduced upon the model line shape analysis. This was performed for all samples, as described above for sample 5, and Table I contains results for layer thickness, and the substrate free-carrier parameters. The $GaInP_2$ phonon mode frequencies are discussed below.

B. Lattice modes in $GaInP_2$

Figure 7 and 8 summarize all E(TO,LO) and A_1(TO,LO) phonon mode frequencies for the $GaInP_2$ samples studied in this work obtained from the fir-SE analysis as a function of η, respectively. We also included recently published values for phonon modes in random and perfectly CuPt-ordered $GaInP_2$ which were calculated using first-principles density-functional linear-response theory.[16,17] The phonon mode frequencies obtained for the sample with $\eta\sim0$ are in very good agreement with our previous mode assignment for highly disordered $GaInP_2$.[7] The disordered alloy exhibits two main bands. One strong InP- and one weak GaP-like band (shaded regions in Fig. 7). We characterize the observed GaP-, and InP-like phonon bands as function of η as follows.

E-type phonon modes (see Fig. 7):

(i) The TO-LO splitting of the GaP-like band (I) decreases with in increasing η.

(ii) The InP-like band splits into tree TO-LO subbands (II), (III), and (IV); band (IV) reveals an extremely small TO-LO splitting for $\eta=0.47$.

A_1-type phonon modes (see Fig. 8): The A_1(TO,LO) phonon modes are identical to the E(TO,LO) phonon modes for the disordered alloy (sample 1), thus reflecting its isotropic character. With increasing η

(i) The TO-LO splitting of the GaP-like band (I) decreases slightly compared with the E-type band. The blueshift of GaP-like A_1(LO) mode is $\Delta\omega\sim4.8$ cm^{-1} for the most ordered sample ($\eta=0.47$).

(ii) The InP-like phonon band also splits into three subbands (II), (III), and (IV). For $\eta\sim0.47$ bands (II) and (III) are well separated, and band (IV) still present.

In addition to the GaP- and InP-like modes, three anisotropic pairs of low-polarity modes AM_1, AM_2, and AM_4 are identified near $\omega\sim312$, ~336, and ~351 cm^{-1}, respectively. For $\eta\sim0$, all modes are isotropic. With increasing η their dependencies can be summarized as follows:

E-type AM modes (see Fig. 7).

(i) AM_1(TO) shifts from $\omega\sim310$ to 316 cm^{-1}, and its TO-LO splitting increases from $\Delta\omega\sim0$ to 8 cm^{-1} for $\eta\sim0-0.47$.

(ii) AM_2 is located at $\omega\sim348$ cm^{-1} independent of η, and its TO-LO splitting is very small for all five samples.

(iii) A second mode occurs within the InP-like phonon band, called here AM_4 to keep consistency with our previous assignment.[7] Its TO frequency is shifted from $\omega\sim336$ to 332 cm^{-1} for $\eta\sim0-0.47$, while its TO-LO splitting increases. For $\eta=0.47$ the gap mode AM_4 nearly merges with AM_1 causing the subband (IV) to show an extremely small TO-LO splitting.

A_1-like phonon modes (see Fig. 8).

(i) AM_1(TO) is also shifted to larger wave numbers, but the TO-LO splitting remains smaller than that with an E-type symmetry.

(ii) In contrast to $E(\mathrm{AM}_2)$ the $A_1(\mathrm{AM}_2)$ frequencies shift from $\omega\sim348$ to 352 cm^{-1} for $\eta\sim0$ to 0.47, and the TO-LO splitting increases slightly to ~1.5 cm^{-1}.

(iii) The AM_4(LO) mode is also shifted to smaller wave numbers (from $\omega\sim338$ to 333 cm^{-1}). The TO-LO splitting is increasing with increasing η, but unlike to the *E*-type modes no subband merging occurs here.

The obtained spectral positions of the GaP- and InP-like LO, and the GaP-like TO modes for the highly disordered sample agree well with data reported in the literature. The value for the InP-TO mode ($\omega\sim322$ cm^{-1}) obtained here seems low compared with the data in the literature, which scatter from $\omega\sim325$ to 331 cm^{-1}, but is consistent with our previous ellipsometry measurements on highly disordered $\mathrm{Ga}_{0.52}\mathrm{In}_{0.48}\mathrm{P}$.[7]

The shift of the GaP- and InP-like A_1(LO,TO) and E(LO,TO) modes with increasing η was only seen in Raman scattering spectra for the GaP- and InP-like LO mode, and was already attributed to long-range ordering.[24,25] The observed blue shift in Raman data for the GaP-like LO mode ranges from $\omega\sim1$ to 4.5 cm^{-1}.[22,24,25] Unfortunately, these Raman studies have been carried out in a (001) backscattering geometry only. Because the phonon wave vector **q** in the backscattering geometry is neither parallel nor perpendicular to the ordering axis the symmetry and polar characters of the modes are mixed.[25] Thus it is not yet clear if the shifted LO mode reported in the literature is that of A_1 or E symmetry. Here we find that the GaP-like E(LO) mode remains almost constant while the A_1(LO) mode is blueshifted by approximately 2 cm^{-1}, resulting in the A_1-E(LO) splitting of ~2 cm^{-1} for $\eta=0.47$. Hassine *et al.*[22] observed, in low-temperature Raman scattering measurements very large splitting of the GaP-like LO mode of ~7 cm^{-1}, but this observation has not been reproduced by other groups.

For the InP-like A_1(LO) mode we also observe a blueshift of approximately 2 cm^{-1} while the E_1(LO) mode remains constant resulting in the A_1-E(LO) splitting of ~2 cm^{-1} for $\eta=0.47$. A similar blue shift has also been reported in Refs. 25 and 24, and was attributed to the InP-like E(LO) mode, but since these measurements have been performed in (001) Raman backscattering geometry as well, it cannot be ruled out that the observed peak is due to a mixed A_1-E(LO) vibration. Mode sharpening was observed in polarized Raman scattering measurements for the InP-like TO mode upon ordering. We explain this effect by the rather complex behavior of the InP-like TO mode with increasing η. The slight blueshift of the InP-like TO mode and the redshift of AM_4 with increasing η results in a narrowing and collapsing of the phonon band (*IV*) for A_1 and E symmetries (Figs. 8 and 7).

Some experimental evidence of a previous observation of the AM_1 mode in ordered GaInP_2 exists in the literature. Mintairov and Melehin[23] reported a weak mode at 315 cm^{-1} after a careful Lorentzian line shape analysis of their Raman spectra of ordered GaInP_2. Hassine *et al.*[22] also reported Raman backscattering data on a (001) face, and, although not further discussed by the authors, a weak resonance can be recognized near $\omega\sim315$ cm^{-1} (Fig. 3 in Ref. 22). Further indications of this weak mode can be found in Raman data published by Cheong *et al.*[26] (Fig. 1 in Ref. 26) and Mestres *et al.*[11] [Figs. 2(a) and 3(a) in Ref. 11], but no systematic study of this mode as a function of η was performed prior to the present work.

The AM_2 mode corresponds with the CuPt-ordering induced mode at $\omega\sim354$ cm^{-1}, which was already observed by several groups using Raman scattering and fir reflections and transmissions intensity measurements. However, we observe this mode not only in the ordered samples but, consistent with our previous work, also in the disordered alloy.[7] Note that mode AM_2 is isotropic for $\eta\sim0$, but very anisotropic for $\eta>0$. There is an ongoing controversy in the literature about the assignment of this mode. Furthermore, the magnitude of the observed blue shift of the AM_2 mode ranges between $\Delta\omega\sim1$ cm^{-1} and ~4.5 cm^{-1} for a maximum valence band splitting of $\Delta E_{\mathrm{VBS}}=30$ and 9.6 meV, respectively.[22,25] The very large blueshift $\Delta\omega\sim4.5$ cm^{-1} occurring for the comparative small $\Delta E_{\mathrm{VBS}}=9.6$ meV has only been observed by Hassine *et al.*[22] Different Raman scattering geometries have been used to reveal the symmetry and character of this mode. Now common agreement seems to exist that the Raman peak is caused by an LO mode with A_1-type symmetry. It is however, still unclear whether this mode is polarized along $[\bar{1}11]$ or $[\bar{1}\bar{1}0]$. One can notice in Figs. 7 and 8 that the AM_2 E(TO,LO) and A_1(TO,LO) frequencies reveal different dependencies on η. While the A_1(TO,LO) frequencies blueshift with increasing η by ~4 cm^{-1} the E(TO,LO) frequencies remain almost constant (shift by ~1 cm^{-1}). The TO-LO splitting for the A_1-type frequencies increases to ~1.5 cm^{-1} while the *E*-type TO-LO splitting remains small (~0.5 cm^{-1}). According to our assignment from $\epsilon_{\parallel}$ and $\epsilon_{\perp}$ the polarization of A_1(LO) and A_1(TO) is along $[\bar{1}\bar{1}1]$ and $[110]$, respectively. The previous controversy about the polarization assignment of this mode, derived from Raman measurements, might be due to its comparatively small (~1.5 cm^{-1}) TO-LO splitting, and ambiguous assignment due to the actual breakdown of the trigonal symmetry selection rules because of the partial character of the CuPt-type ordering.

The mode AM_4 located within the InP-like phonon band exhibits a very strong dependency on η, and nearly merges with the InP-like TO mode. For the most ordered sample ($\eta=0.47$) the E(TO,LO) mode splitting vanishes but the A_1(TO,LO) band is still present. Mintairov *et al.*[68] reported the occurrence of a mode at $\omega\sim340$ cm^{-1} in Raman scattering spectra for a sample with $\Delta E_{\mathrm{VBS}}=28$ meV, which might correspond to the mode AM_4.

The AM modes prove to be very sensitive to the degree of ordering η, and it is obvious that these modes contain information on the next neighbor configurations. Moreover, the AM modes although not anisotropic exist also in sample 1 which should not contain any ordered domains according to its band gap value ($E_g=1.899$ eV at 300 K).[69] However, the existence of residual ordering, too small to affect the band gap but appreciable enough to affect local bond vibrations, cannot be ruled out either. CuPt ordering seems to activate the AM modes for Raman scattering. The A_1-E splitting for

the GaP- and InP-like phonon modes are small compared to their LO-TO splitting, i.e., the long-range electrostatic forces dominate over the anisotropic short-range forces. However, for the alloy-induced modes we observe a stronger dependence on the ordering parameter, and their A_1-E splitting is comparable to the TO-LO splitting. Hence, for AM modes, the anisotropic short-range forces should dominate over the long-range electrostatic forces.

Ozoliņš and Zunger calculated the phonon spectra of $GaInP_2$ using first-principles density-functional linear-response theory and predicted splitting of the GaP- and InP-like phonon bands with A_1 and E symmetry. So far, it was unknown how the splitting will emerge for partial ordering.[16,17] Ozoliņš and Zunger suggested the application of the "η^2 rule," in which strength and spectral position should scale with η^2 times the difference of the respective quantity (strength and position) imposed upon perfect order or disorder. The AM_1 mode with E symmetry and the AM_2 mode with A_1 symmetry seem to match the dispersionless E(TO) mode, predicted at 316 cm^{-1} and the CuPt-order-induced mode of A_1 symmetry at $\sim$350 cm^{-1}. However, the GaP- and the InP-like modes observed here fit only partially within the mode picture predicted by Ozoliņš and Zunger. At this point, and from the η range studied here, it remains unclear whether the "η^2 rule" is applicable or not, because the experimental determination of $\epsilon(\eta=1)$ is still lacking.

V. SUMMARY

A fir ellipsometric study of spontaneously ordered $GaInP_2$ thin films with degrees of ordering $0\sim\eta\leqslant 0.47$ was performed. The exactly determined anisotropic fir dielectric functions provide a link between the fir optical sample response and the fir-active phonon modes. The phonon mode frequencies of $GaInP_2$ are presented as a function of η. For $\eta\sim 0$ we identify GaP- and InP-like phonon modes, and three alloy-induced modes (AM_1, AM_2, and AM_4) with low polarity. These modes shift and split in E- and A_1-type vibrations with increasing η. The change of the GaP- and InP-like modes upon ordering is weak confirming previous indications from Raman scattering experiments. The alloy-induced modes are distinctly affected by η. For example, the mode AM_2 produces strong fir anisotropy for wave numbers near $\omega\sim 354$ cm^{-1} due to the increase of the $A_1(AM_2)$ TO-LO and AM_2(TO) E-A_1 splitting with increasing η where the $E_1(AM_2)$ TO-LO splitting remains small. The identified mode behavior allows the assignment of the ordering-induced mode previously observed at this wave number in Raman scattering and fir spectroscopy as an LO mode with A_1-type symmetry. We suggest that the ordered arrangement of alike group-III atoms in common sublattices is the possible physical mechanism for the occurrence of the alloy-induced modes, where strength (TO-LO splitting) and anisotropy (E-A_1 splitting) may scale with the degree of ordering η.

We propose the alloy-induced modes as sensible measure for the degree of ordering in indirect multinary alloys where typical optical order-fingerprints such as band splitting values cannot be easily obtained. We expect the observation of very similar mode behavior in multinary alloys with other than the CuPt-type ordering.

ACKNOWLEDGMENTS

The authors acknowledge Daniel Thompson, University of Nebraska at Lincoln, for technical support of the work. We thank Professor Wolfgang Grill (UL), Professor Marius Grundmann (UL), Professor Woollam (UNL), and B. Rheinländer (UL) for continuing support of our work. Financial support for this study was provided in part by CMOMR at UNL, NSF Contract No. DMI-9901510, and DFG Contract No. Rh28/3-2.

*Electronic address: Tino. Hofmann@physik.uni-leipzig.de
†Electronic address: mschub@physik uni-leipzig.de; URL: http://www.uni-leipzig.de~hlp/ellipsometrie

[1] D. Bimberg *et al.*, in *Numerical Data and Functional Relationships in Science and Technology*, edited by O. Madelung, Landolt-Bornstein, New Series, Group 1, Vol. XIIV, Pt. a.
[2] G. Lucovsky, M.H. Brodsky, M.F. Chen, R.J. Chicotka, and A.T. Ward, Phys. Rev. B **4**, 1945 (1971).
[3] B. Jusserand and S. Slempkes, Solid State Commun. **49**, 95 (1984).
[4] T. Kato, T. Matsumoto, and T. Ishida, Jpn. J. Appl. Phys. Part 1 **27**, 983 (1988).
[5] M. Kondow, S. Minagawa, and S. Satoh, Appl. Phys. Lett. **51**, 2001 (1987).
[6] M. Kubo, M. Mannoh, Y. Takahashi, and M. Ogura, Appl. Phys. Lett. **52**, 715 (1988).
[7] T. Hofmann, G. Leibiger, V. Gottschalch, I. Pietzonka, and M. Schubert, Phys. Rev. B **64**, 155206 (2001).
[8] F. Alsina, J.D. Webb, A. Mascarenhas, J.F. Geisz, J.M. Olson, and A. Duda, Phys. Rev. B **60**, 1484 (1999).
[9] E. Jahne, W. Pilz, M. Giehler, and L. Hildisch, Phys. Status Solidi B **91**, 155 (1979).
[10] H. Asahi, S. Emura, and S. Gonda, J. Appl. Phys. **65**, 5007 (1989).
[11] N. Mestres, F. Alsina, J. Pascual, J.M. Bluet, J. Camassel, C. Geng, and F. Scholz, Phys. Rev. B **54**, 17 754 (1996).
[12] F. Alsina, H.M. Cheong, J.D. Webb, A. Mascarenhas, J.F. Geisz, and J.M. Olson, Phys. Rev. B **56**, 13 126 (1997).
[13] R. M. Azzam and N. M. Bashara, *Ellipsometry and Polarized Light* (North-Holland, Amsterdam, 1977).
[14] E. Jellison, Thin Solid Films **313/314**, 33 (1998).
[15] A. Zunger, MRS Bull. **22**, 20 (1997).
[16] V. Ozoliņš and A. Zunger, Phys. Rev. B **57**, R9404 (1998).
[17] V. Ozoliņš and A. Zunger, Phys. Rev. B **63**, 087202 (2001).
[18] F. Alsina, N. Mestres, A. Nakhli, and J. Pascual, Phys. Status Solidi B **215**, 121 (1999).
[19] K. Sinha, A. Mascarenhas, G.S. Horner, R.G. Alonso, K.A. Bertness, and J.M. Olson, Phys. Rev. B **48**, 17 591 (1993).
[20] K. Sinha, A. Mascarenhas, G.S. Horner, K.A. Bertness, S.R. Kurtz, and J.M. Olson, Phys. Rev. B **50**, 7509 (1994).
[21] A. Mintairov, B. Zvonkov, T. Babushkina, I. Malkina, and Y. Saf'yano, Fiz. Tverd. Tela (Leningrad) **37**, 3607 (1995) [Phys. Solid State **37**, 1985 (1995)].

[22] A. Hassine, J. Sapriel, P. Le Berre, M.A. Di Forte-Poisson, F. Alexandre, and M. Quillec, Phys. Rev. B **54**, 2728 (1996).
[23] A. Mintairov and V. Melehin, Semicond. Sci. Technol. **11**, 904 (1996).
[24] F. Alsina, N. Mestres, J. Pascual, C. Geng, P. Ernst, and F. Scholz, Phys. Rev. B **53**, 12 994 (1996).
[25] H.M. Cheong, A. Mascarenhas, P. Ernst, and C. Geng, Phys. Rev. B **56**, 1882 (1997).
[26] H.M. Cheong, F. Alsina, A. Mascarenhas, J.F. Geisz, and J.M. Olson, Phys. Rev. B **56**, 1888 (1997).
[27] H.M. Cheong, A. Mascarenhas, J.F. Geisz, and J.M. Olson, Phys. Rev. B **62**, 1536 (2000).
[28] E. Jahne, A. Röseler, and K. Ploog, Proc. SPIE **1575**, 277 (1991).
[29] E. Wold, J. Bremer, O. Hunderi, and B.-O. Fimland, Thin Solid Films **313-314**, 649 (1998).
[30] J. Humlíček, R. Henn, and M. Cardona, Phys. Rev. B **61**, 14 554 (2000).
[31] T.E. Tiwald, J.A. Woollam, S. Zollner, J. Christiansen, R.B. Gregory, T. Wetteroth, S.R. Wilson, and A.R. Powell, Phys. Rev. B **60**, 11 464 (1999).
[32] S. Zangooie, M. Schubert, D. Thompson, and J. Woollam, Appl. Phys. Lett. **78**, 937 (2001).
[33] A. Kasic, M. Schubert, S. Einfeldt, D. Hommel, and T. Tiwald, Phys. Rev. B **62**, 7365 (2000).
[34] A. Kasic, M. Schubert, B. Kuhn, F. Scholz, S. Einfeldt, and D. Hommel, J. Appl. Phys. **89**, 3720 (2001).
[35] A. Barker, Jr. and A. Sievers, Rev. Mod. Phys. **47**, FS1 (1975).
[36] C. Pidgeon, in *Handbook on Semiconductors*, edited by M. Balkanski (North-Holland, Amsterdam, 1980), Vol. 2, pp. 223–328.
[37] P. Yu and M. Cardona, *Fundamentals of Semiconductors* (Springer-Verlag, Berlin, 1999).
[38] F. Gervais and B. Piriou, J. Phys. C **7**, 2374 (1974).
[39] D. Berreman and F. Unterwald, Phys. Rev. **174**, 791 (1968).
[40] A.A. Kukharskii, Solid State Commun. **13**, 1761 (1973).
[41] E. Burnstein, A. Hartstein, J. Schoenwald, A. Maradudin, D. Mills, and R. Wallis, in *Polaritons*, edited by E. Bunstein and F. de Martini (Pergamon, New York, 1974), P. 89.
[42] J. Humlíček, R. Henn, and M. Cardona, Appl. Phys. Lett. **69**, 2581 (1996).
[43] A. Kasic, M. Schubert, Y. Saito, Y. Nanishi, and G. Wagner, Phys. Rev. B **65**, 115206 (2002).
[44] G. Leibiger, V. Gottschalch, A. Kasic, and M. Schubert, Appl. Phys. Lett. **79**, 3407 (2001).
[45] A. Kasic, M. Schubert, J. Off, and F. Scholz, Appl. Phys. Lett. **78**, 1526 (2001).
[46] W. Press, B. Flannery, S. Teukolsky, and W. Vetterling, *Numerical Recipes: The Art of Scientific Computing* (Cambridge University Press, Cambridge, 1988).
[47] M. Schubert, T.E. Tiwald, and C.M. Herzinger, Phys. Rev. B **61**, 8187 (2000).
[48] The equations developed for the partial transfer matrix $\mathbf{T}_p$ of CuPt-ordered films in Ref. 58 are not valid for $\epsilon_{\|}, \epsilon_{\perp}$ in the fir spectral region. The linearization in $\Delta\epsilon$ (see Appendix A in Ref. 58) is not correct here because the presumption $\Delta\epsilon \ll \epsilon$ is not fulfilled anymore. The exact equations for $\mathbf{T}_p$ given in Ref. 63 are therefore used for data analysis in the fir.
[49] Model parameters for GaAs were obtained from fir-SE analysis of bare substrates with metal-organic-vapor-phase-epitaxy grown GaAs buffer layers. Values for ω_{TO}, ω_{LO}, γ_{TO}, γ_{LO}, and ϵ_{∞} were highly consistent within several samples and were not further varied here.
[50] S.H. Wei and A. Zunger, Phys. Rev. B **39**, 3279 (1989).
[51] S.-H. Wei and A. Zunger, Phys. Rev. B **49**, 14 337 (1994).
[52] P. Ernst, C. Geng, F. Scholz, H. Schweizer, Y. Zhang, and A. Mascarenhas, Appl. Phys. Lett. **67**, 2347 (1995).
[53] M. Schubert, B. Rheinländer, and V. Gottschalch, Solid State Commun. **95**, 723 (1995).
[54] S.-H. Wei, D.B. Laks, and Z. Alex, Appl. Phys. Lett. **62**, 1937 (1993).
[55] S.-H. Wei and A. Zunger, Phys. Rev. B **57**, 8983 (1998).
[56] K.A. Mäder and A. Zunger, Appl. Phys. Lett. **64**, 2882 (1994).
[57] K.A. Mäder and A. Zunger, Phys. Rev. B **51**, 10 462 (1995).
[58] M. Schubert, T. Hofmann, B. Rheinländer, I. Pietzonka, T. Saß, V. Gottschalch, and J.A. Woollam, Phys. Rev. B **60**, 16 618 (1999).
[59] M. Schubert, B. Rheinländer, E. Franke, I. Pietzonka, J. Škriniarová, and V. Gottschalch, Phys. Rev. B **54**, 17 616 (1996).
[60] M. Schubert, Thin Solid Films **313-314**, 323 (1998).
[61] For these sample orientations, the off-diagonal Jones reflection matrix elements are zero (setup $\mathcal{A}$) or very small ($\mathcal{B}$). Hence one can avoid the full generalized ellipsometry procedure, where the sample response to multiple incident polarization states needs to be mapped out to find the three complex ratios R_{pp}, R_{ps}, and R_{sp}. Instead, the normal ellipsometry parameters are determined, which approximate R_{pp}, and R_{ps}, R_{sp} are neglected. For a thorough discussion and presentation of the generalized ellipsometry see Refs. 58 and 60 and references therein.
[62] D.W. Berreman, Phys. Rev. **130**, 2193 (1963).
[63] M. Schubert, Phys. Rev. B **53**, 4265 (1996).
[64] J. Šik, M. Schubert, T.E. Tiwald, and T. Hofmann, MRS Internet J. Nitride Semicond. Res. **4**, 11 (2000).
[65] A. Röseler, *Infrared Spectroscopic Ellipsometry* (Akademie-Verlag, Berlin, 1990).
[66] This resonance effect is related to the excitation of an interface-bound Fano-type surface polariton, following the notation given in Ref. 41. A thorough discussion of this phenomenon in semiconductor heterostructures will be given somewhere else.
[67] The observed alloying modes were indexed in consistency with our previous work on highly disordered AlGaInP (Ref. 7).
[68] A.M. Mintairov, P.A. Blagnov, V.G. Melehin, N.N. Faleev, J.L. Merz, Y. Qiu, S.A. Nikishin, and H. Temkin, Phys. Rev. B **56**, 15 836 (1997).
[69] M. Schubert, J.A. Woollam, G. Leibiger, B. Rheinländer, I. Pietzonka, T. Saß, and V. Gottschalch, J. Appl. Phys. **86**, 2025 (1999).